Sustainable Food Technology

ROYAL SOCIETY OF CHEMISTRY

PAPER

View Article Online
View Journal

Cite this: DOI: 10.1039/d5fb00462d

Plasma-assisted modification of micronutrient-embedded PVA/PVP blend films for sustained nutrient delivery in agricultural applications

Nandhu Varshini Gnanasekar and Shanmugavelayutham Gurusamy *

Sustained and controlled delivery of micronutrients remains a critical challenge in agricultural systems, largely due to the high solubility and uncontrolled release of conventional polymer-based nutrient carriers. In this work, we report for the first time the use of non-thermal Dielectric Barrier Discharge (DBD) plasma to modify PVA/PVP-based films embedded with $CuSO_4$ and $FeSO_4$, aiming to enhance their performance for controlled nutrient release applications. The composite films synthesized by the solution casting method were subjected to argon plasma treatment at 25 kV for various exposure durations. Physicochemical characterization and mechanical properties confirmed the notable surface changes after plasma exposure such as increased roughness, formation of oxygen functional groups, plasma-induced crosslinking and increased tensile strength. These modifications contributed to the formation of a denser film network, effectively slowing ion diffusion. *In vitro* nutrient release studies showed a reduction in the release rate of Cu^{2+} ions, decreasing from 85.4 ± 1.8% to 49.4 ± 1.4% after plasma treatment. Kinetic modeling indicated that the release behavior followed the Higuchi model, suggesting a diffusion-controlled mechanism influenced by the altered film structure. This work presents a novel and eco-friendly approach for engineering polymer–metal salt films *via* plasma technology, demonstrating strong potential for sustained micronutrient delivery in agricultural applications.

Received 6th August 2025
Accepted 18th October 2025

DOI: 10.1039/d5fb00462d

rsc.li/susfoodtech

Sustainability spotlight

While polymer-based delivery systems have been widely studied in pharmaceuticals, their application in agriculture, particularly for micronutrient delivery, remains limited. This study presents plasma-treated PVA/PVP films embedded with $CuSO_4$ and $FeSO_4$ salts as a proof-of-concept system for controlled micronutrient release. Non-thermal plasma treatment provides a chemical-free method to tailor surface properties and release behavior, positioning it as a promising approach for sustainable agricultural practices. Although PVA and PVP are synthetic polymers with limited biodegradability, they offer a reliable and well-characterized platform to systematically investigate plasma–polymer interactions. Importantly, these results pave the way for applying plasma treatment to bio-based, biodegradable polymer systems to achieve efficient nutrient release with lower environmental impact.

1 Introduction

Agricultural productivity in developing countries faces numerous constraints, with one of the most critical being the insufficient availability of essential nutrients in appropriate forms and quantities. For better plant growth, a controlled and balanced supply of both macronutrients and micronutrients is essential. These nutrients play a fundamental role in plant metabolism and directly influence the crop yield potential.[1,2] In recent agricultural practices, farmers have largely concentrated on the application of macronutrients, with limited attention given to the role of micronutrients. Moreover, the availability of these micronutrients in soil has become increasingly restricted due to their continuous depletion from repeated and intensive cultivation practices.[3] Micronutrients are commonly supplied as soluble salts, particularly in the form of sulfates such as ferrous sulfate ($FeSO_4$), copper sulfate ($CuSO_4$), manganese sulfate ($MnSO_4$), and zinc sulfate ($ZnSO_4$). Chelated compounds are also frequently used to enhance the availability of iron. Additionally, potassium chloride is applied as a chlorine source, while boron and molybdenum are provided through borax and sodium molybdate, respectively.[4] However, the conventional fertilization approaches are associated with several limitations, including rapid leaching, low bioavailability, poor uptake efficiency and frequent dosing requirements to maintain adequate nutrient levels in the soil. Also, the inefficient delivery and poor uptake of these micronutrients continue to pose a major challenge in achieving sustainable crop production. To address these issues, nowadays, there is a growing interest in controlled-release systems that can deliver micronutrients in a sustained manner. Among the various carrier materials available for

Plasma Physics and Processing Laboratory, Department of Physics, Bharathiar University, Coimbatore-641 046, Tamil Nadu, India. E-mail: sgsvelu@buc.edu.in

controlled release, polymer-based systems have gained prominence due to their versatility, structural stability and ability to tailor release profiles.[5,6] Polyvinyl alcohol (PVA) and polyvinylpyrrolidone (PVP) are widely used polymers in pharmaceutical and agricultural applications because of their non-toxicity, excellent film-forming properties and strong compatibility with a wide range of additives. When blended, PVA and PVP form flexible films with good mechanical properties, making them suitable candidates for use as micronutrient delivery matrices.[7–9] Copper (Cu) and iron (Fe) are essential micronutrients that play critical roles in various physiological and biochemical processes in plants. Copper is vital for lignin synthesis, photosynthetic electron transport, and enzymatic activities involved in oxidative stress tolerance, while iron is indispensable for chlorophyll synthesis, respiration, and energy transfer processes.[10,11] Among the various available sources, $CuSO_4$ and $FeSO_4$ were selected for incorporation as micronutrients within the PVA/PVP blend films.

To enhance the functional performance of these polymer blends, surface modification is essential. In agricultural applications, functional performance refers to the ability of polymer films to interact with water and soil, encapsulate nutrients within the matrix during film formation, and release them in a controlled and sustained manner. Surface modification plays a critical role in this process by improving surface properties such as hydrophilicity, roughness, surface energy and crosslinking. Currently, non-thermal plasma surface treatment is widely employed as an effective, single-step, chemical-free and environmentally friendly approach to modify the surface characteristics without altering the bulk properties of the material.[12–15] During plasma treatment, energetic species such as ions, electrons, ultraviolet photons, and reactive oxygen and nitrogen species (RONS) interact with the polymer surface, leading to bond scission, crosslinking and the introduction of new polar functional groups. The free radicals and reactive sites generated can recombine or react with atmospheric species to form covalent bonds, producing a denser network. The resulting tighter network restricts polymer chain mobility, limits diffusion pathways and slows nutrient release into the medium. This controlled release prevents rapid leaching and prolongs nutrient availability, ensuring a more regulated supply of micronutrients from the polymer films. Meanwhile, the incorporation of polar functional groups enhances surface wettability, enabling faster initial water uptake, while crosslinking regulates the sustained release. Although plasma-treated polymer films hold significant potential for agricultural use, their application in micronutrient delivery remains largely unexplored. Therefore, understanding the influence of plasma treatment time on film properties and nutrient release profiles is essential for optimizing these systems for agricultural applications.

In this study, we investigate the impact of plasma treatment time on the controlled release of micronutrients ($CuSO_4$ and $FeSO_4$) from PVA/PVP blend films. By varying the plasma treatment time, we aim to correlate the surface modifications with changes in the surface properties and micronutrient release profiles. The findings of this work could contribute to the long-term micronutrient availability in agricultural applications.

2 Materials and methods

2.1. Materials

Polyvinyl alcohol (PVA), polyvinylpyrrolidone (PVP), copper sulfate ($CuSO_4 \cdot 5H_2O$) and ferrous sulfate ($FeSO_4 \cdot 7H_2O$) with the molecular weights of 160 000 g mol^{-1}, ~40 000 g mol^{-1}, 249.69 g mol^{-1} and 278.01 g mol^{-1} were purchased from Himedia Laboratory Private Ltd, Maharashtra, India. Argon gas with 99% purity was supplied by Sri Venkateswara gas agency, Coimbatore, India.

2.2. Preparation of $CuSO_4$ and $FeSO_4$ embedded PVA/PVP blend films

Initially, 5 g of PVA was dissolved in 50 ml of distilled water and simultaneously, 5 g of PVP was dissolved in a separate 50 ml of distilled water. Both solutions were stirred individually at 500 rpm for 24 hours to ensure complete dissolution. Subsequently, the two polymer solutions were combined and further stirred for an additional 24 hours at 500 rpm to achieve a homogeneous blend. Following this, 1 wt% of $CuSO_4$ was added to the mixture and stirred continuously for 2 hours. A similar procedure was followed for preparing $FeSO_4$-loaded films. The final solutions were then cast into Petri plates and dried in an oven at 50 °C for 48 hours. After drying, the films were stripped off, cut into 2 cm × 2 cm dimensions, and stored in a desiccator for further characterization analysis. The thickness of the synthesized films was measured using a digimatic micrometer (Mitutoyo) and found to be 0.232 ± 0.015 mm.

2.3. Experimental setup of DBD plasma

The experimental setup and the photographic images of the Dielectric Barrier Discharge (DBD) plasma system are shown in Fig. 1 and S1. The system consists of two parallel copper electrodes, each covered with a dielectric barrier to prevent arc formation and ensure uniform plasma discharge. The electrodes were connected to a high-voltage power supply to generate the plasma. During treatment, the film samples were placed between the electrodes within the plasma chamber. To create the plasma environment, process gases were introduced into the chamber, and the gas flow rate was precisely regulated using a gas flow meter to maintain stable discharge conditions.

2.4. Plasma treatment on polymer films

The synthesized PVA/PVP/$CuSO_4$ and PVA/PVP/$FeSO_4$ polymer films were subjected to argon DBD plasma treatment to modify their surface properties. The treatments were carried out at a discharge voltage of 25 kV, with exposure durations of 5, 10 and 15 min, to study the effect of plasma duration on film characteristics. During the treatment, the films were placed inside the parallel plate plasma chamber, maintaining a discharge gap of 10 mm. The argon gas flow was maintained at 10 lpm using a gas flow meter to provide a stable plasma environment.

2.5. Characterization techniques

2.5.1. Weight loss and contact angle analysis. To evaluate the effect of plasma treatment on the polymer films, weight loss analysis was performed immediately after the plasma exposure. The film samples were weighed using a high-precision analytical balance (Electronic Balance – SHIMADZU, Model: ATY 224 R) equipped with a windshield and a readability of 0.0001 g, ensuring accurate detection of even minor weight changes in the samples. The percentage weight loss was calculated using the following formula,

$$\text{Weight loss (\%)} = ((W_U - W_P)/W_U) \times 100 \quad (1)$$

where W_U denotes the weight of the films before plasma treatment and W_P denotes the weight of the films after plasma treatment.

The hydrophilicity of the untreated and plasma-treated samples was evaluated by measuring the contact angle using the sessile drop method with a Goniometer (HO-IAD-CAM-01B, Holmarc, India). Distilled water was used as the probing liquid and each measurement was performed in triplicate to ensure accuracy. The surface energy of all the samples was calculated using the equation,[12]

$$\text{S. E (water)} = 2.9 \times 10^5(\theta)^3 - 0.00652(\theta)^2 - 0.1326(\theta) + 72.8 \text{ mJ m}^{-2} \quad (2)$$

where θ represents the measured contact angle (in degrees).

Additionally, aging studies were performed to evaluate the hydrophobic recovery behavior of the plasma-treated films over time. The water contact angle of the film was measured on the 7th day after plasma treatment to evaluate the changes in surface wettability during the aging process.

2.5.2. ATR-FTIR and XPS analysis. The chemical functional groups of the untreated and plasma-treated films were analyzed using Attenuated Total Reflectance-Fourier Transform Infrared Spectroscopy (ATR-FTIR) analysis (JASCO FT/IR-4700). The measurements were conducted at atmospheric pressure and the spectra were recorded in the wavenumber range of 4000 cm^{-1} to 400 cm^{-1}. Further, the changes in the surface chemical composition and binding energies due to plasma treatment were investigated using X-ray Photoelectron Spectroscopy (XPS) analysis (Thermo Scientific, Alpha-KAN995413) equipped with a monochromatic Al Kα X-ray source ($h\nu = 1486.6$ eV) with the power of 72 W (12 kV and 6 mA). The data was recorded using Avantage 5 software.

2.5.3. SEM and AFM analysis. The surface morphology of the plasma-treated polymer films was examined using Scanning Electron Microscopy (SEM) (FEI-Quanta FEG 250, USA). SEM analysis provided detailed information on the surface topography, texture variations, and morphological changes induced by the plasma treatment. Furthermore, the surface roughness characteristics of the films were quantitatively evaluated using Atomic Force Microscopy (AFM) (Prima, NTEGRA, NT-MDT, Russia). The average surface roughness (R_a) values determined from AFM analysis gives detailed insight into the nanoscale topographical changes resulting from the plasma exposure.

2.5.4. Degree of crosslinking and mechanical properties. The degree of crosslinking of the plasma-treated films was assessed through a gravimetric method based on water insolubility. The films were immersed in distilled water and allowed to soak for 24 days at room temperature. After the soaking period, the resulting solution was filtered using Whatman No. 1 filter paper. The filter paper containing the crosslinked polymer was then dried in a hot air oven at 50 °C for 24 hours. Subsequently, the dried filter paper was weighed to determine the mass of the retained crosslinked polymer. The degree of crosslinking was determined using the equation,

$$\text{Degree of crosslinking (\%)} = ((M_2 - M_1)/M) \times 100 \quad (3)$$

where M_1 is the initial weight of the filter paper, M_2 is the final weight of the filter paper after drying and M is the original dry weight of the polymer films.

The tensile properties of the untreated and plasma-treated polymer films (15 minutes exposure) were measured according to the method of ASTM D882-01,[16] using a Zwick Roell Universal Strength Tester Machine-5KN (Zwick Roell, Germany) at 25 °C. The rectangular film specimens (20 mm × 10 mm) were tested with an initial grip separation of 20 mm and a deformation speed of 12 mm min^{-1}.

2.5.5. Nutrient release test. The *in vitro* nutrient release behavior of both untreated and plasma-treated films was evaluated by immersing the samples in 10 ml of distilled water and placing them in an incubator shaker at 25 rpm. At predetermined time intervals, aliquots of the release medium were withdrawn and immediately replaced with an equal volume of fresh water. The absorbance of the collected samples was measured using UV-Visible spectroscopy (MAR-SPEC DT 3000) (SpectraSuite software) at 813 nm for $CuSO_4$ and 295 nm for $FeSO_4$. The cumulative release percentage of each micronutrient from the films was calculated based on the corresponding standard calibration curves of $CuSO_4$ and $FeSO_4$ solutions.

2.5.6. Nutrient release kinetics. The release behavior of nutrients from the synthesized polymer films was evaluated by fitting the experimental data to well-established kinetic models commonly used in drug delivery and controlled release studies. The applied models included zero-order, first-order, Higuchi and Korsmeyer–Peppas equations, which describe different release mechanisms such as constant release, concentration-dependent release, diffusion-controlled release and anomalous transport, respectively.

The cumulative nutrient release (%) over time was calculated and fitted to the respective linearized forms of the models as per the literature:[17]

$$\text{Zero-order: } Q = k_0 \cdot t$$

$$\text{First-order: } \log C = \log C_0 - kt/2.303$$

$$\text{Higuchi: } Q = kt^{1/2}$$

$$\text{Korsmeyer–Peppas: } M_t/M_g = kt^n$$

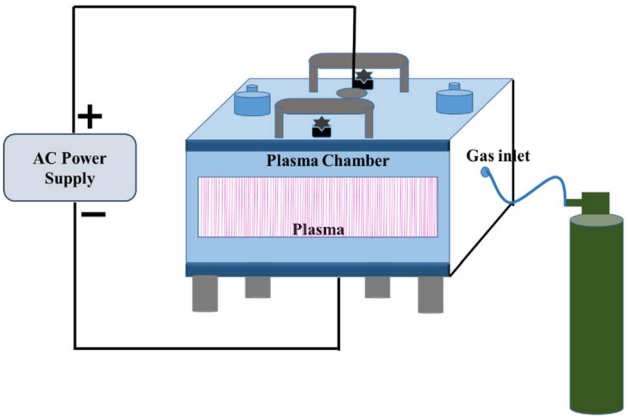

Fig. 1 Schematic representation of DBD plasma system.

Here, Q is the cumulative amount of nutrient released at time t, C_0 is the initial concentration of the nutrient and k is the release rate constant. For the Korsmeyer–Peppas model, the exponent n indicates the release mechanism (Fickian, non-Fickian or case II transport).

2.5.7. Statistical analysis. All experimental measurements were statistically analyzed by calculating the mean values and their corresponding standard deviations. One-way analysis of variance (ANOVA) was performed to compare the data across different sample groups, with a significance level of $p < 0.05$ used to identify statistically meaningful differences.

3 Results and discussion

3.1. Weight loss analysis

The effect of plasma treatment on the weight loss behavior of PVA/PVP/$CuSO_4$ and PVA/PVP/$FeSO_4$ polymer films was investigated by measuring the weight of the polymer films immediately after plasma exposure. As illustrated in the Fig. 2, the weight loss percentage increases progressively with increasing plasma treatment time for both films. This can be attributed to the plasma-induced surface etching and functionalization processes. During plasma treatment, high-energy ions, electrons, UV photons and reactive radicals interact with the polymer surface. This interaction leads to the removal of surface-bound impurities, low-molecular weight residues and loosely attached polymer chains, resulting in a measurable reduction in the weight of the films.[18] Notably, PVA/PVP/$CuSO_4$ films exhibited higher weight loss compared to the PVA/PVP/$FeSO_4$ films, suggesting a difference in surface response under plasma conditions. The highest weight loss was observed at 15 minutes of treatment, where the weight loss was 0.99% and 0.84% for $CuSO_4$ and $FeSO_4$ films, respectively. These results demonstrates that the plasma treatment effectively alters the surface characteristics of the polymer films.

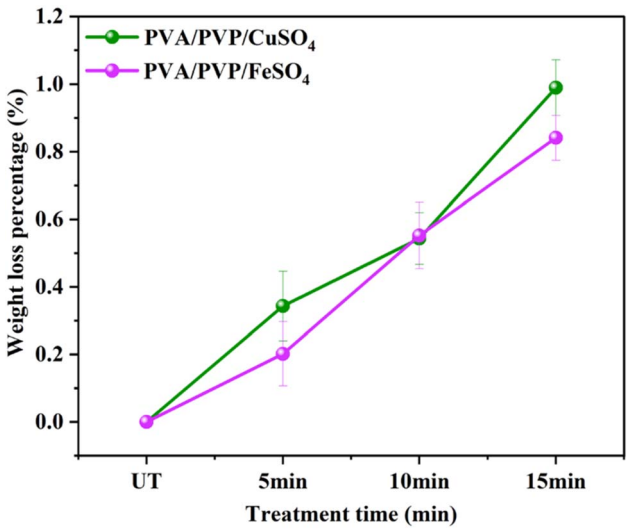

Fig. 2 Weight loss analysis of polymer films after plasma treatment.

3.2. Contact angle analysis

The contact angle measurements and corresponding surface energy values of the PVA/PVP/$CuSO_4$ and PVA/PVP/$FeSO_4$ composite films are illustrated in Fig. 3a and b. As shown in Fig. 3a, the untreated PVA/PVP/$CuSO_4$ films exhibited a contact angle of 69.9° ± 2.9°, indicating moderate surface hydrophilicity. Upon plasma treatment, a progressive reduction in contact angle was observed with increasing treatment duration, reaching a minimum value of 50.1° ± 3.9° after 15 minutes of exposure. Correspondingly, the surface energy of the films increased from 41.5 ± 2.9 mJ m^{-2} in the untreated films to 53.4 ± 3.9 mJ m^{-2} after 15 minutes plasma treatment, further confirming the increased surface activation and wettability. Similarly, Fig. 3b presents the contact angle data for the PVA/PVP/$FeSO_4$ films. The untreated films showed a higher initial contact angle of 76.8° ± 1.9°, which decreased to 52.3° ± 1.9° after 15 minutes of plasma exposure. In parallel, the surface energy improved from 37.2 ± 1.9 mJ m^{-2} to 52.1 ± 1.9 mJ m^{-2}. These findings demonstrate that plasma treatment effectively alters the surface characteristics of the polymer films by increasing their hydrophilicity and surface energy, primarily through plasma-induced surface oxidation and incorporation of polar functional groups.

3.3. Aging analysis

The aging behavior of the plasma-treated PVA/PVP/$CuSO_4$ and PVA/PVP/$FeSO_4$ composite films was investigated by measuring the contact angle on the 7th day after plasma exposure, as illustrated in Fig. 4a and b. All the plasma-treated samples exhibited a slight increase in contact angle after 7 days, indicating a gradual reduction in surface hydrophilicity over time. Also, no further significant changes were observed beyond the 7th day, suggesting stabilization of the surface characteristics. For the PVA/PVP/$CuSO_4$ films treated for 15 minutes, the contact angle increased from 50.1° ± 3.9° (immediately after treatment) to 53.7° ± 1.6° on the 7th day. Similarly, in the case of PVA/PVP/$FeSO_4$ films, the contact angle rises from 52.3° ± 1.9° to 56.6° ± 1.8° over the same period. This increase in contact angle is attributed to hydrophobic recovery which is commonly observed in plasma-treated polymers, resulting from

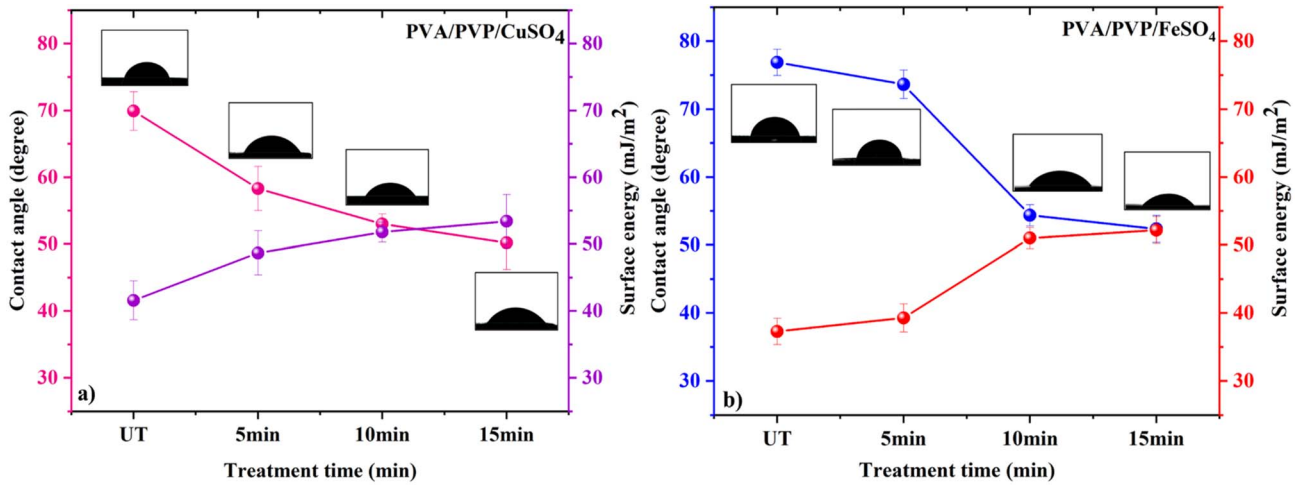

Fig. 3 Contact angle analysis of (a) PVA/PVP/$CuSO_4$ and (b) PVA/PVP/$FeSO_4$ polymer films.

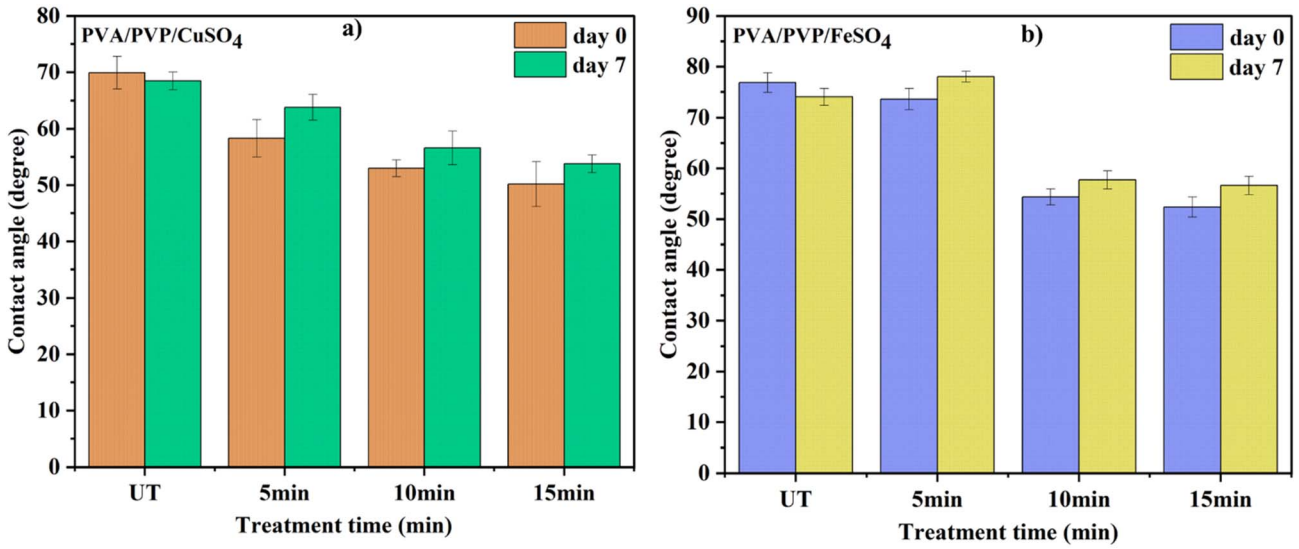

Fig. 4 Aging analysis of (a) PVA/PVP/$CuSO_4$ and (b) PVA/PVP/$FeSO_4$ polymer films.

the reorientation or migration of polar functional groups towards the bulk material. Despite this slight increase in contact angle, the aged films did not revert to their original untreated contact angle values, indicating that the plasma-induced modifications are stable and retain a degree of surface activation over time.[19]

3.4. FTIR analysis

The chemical functional groups of the PVA/PVP/$CuSO_4$ and PVA/PVP/$FeSO_4$ composite films and their changes after plasma treatment were examined using FTIR analysis, as shown in Fig. 5a and b.

Fig. 5a presents the FTIR spectra of untreated and plasma-treated PVA/PVP/$CuSO_4$ films, while Fig. 5b shows the corresponding spectra for PVA/PVP/$FeSO_4$ films. In both cases, a broad absorption band is observed in the range of 3585–3057 cm^{-1} ($CuSO_4$) and 3571–3099 cm^{-1} ($FeSO_4$) is attributed to the O–H stretching vibrations of hydroxyl groups in PVA.[20] The peaks located at 2946, 2904 cm^{-1} ($CuSO_4$), and 2943, 2902 cm^{-1} ($FeSO_4$) correspond to the C–H stretching vibrations of PVA.[21] A distinct absorption band around 1728 cm^{-1} ($CuSO_4$) and 1730 cm^{-1} ($FeSO_4$) is ascribed to the carbonyl groups of residual acetate moieties in the PVA.[22] Furthermore, a peak at 1646 cm^{-1} ($CuSO_4$) and 1643 cm^{-1} ($FeSO_4$) is attributed to the overlapping of C=O and N–C=O stretching vibrations, reflecting the presence of both PVA and PVP in the film composition.[23,24] Characteristic peaks observed at 1496 cm^{-1} ($CuSO_4$) and 1495 cm^{-1} ($FeSO_4$) represents the CH_2 bending deformation groups from vinyl backbone of PVA and CH_2 bending deformation of linear chain of PVP.[25,26] Additional vibrational bands located at 1439, 1422, 1372, 1288 cm^{-1} in $CuSO_4$-based films and 1435, 1422, 1373, 1286 cm^{-1} in $FeSO_4$-based films are assigned to the scissoring,[27] wagging,[28] bending[29] and twisting modes[28] of CH_2

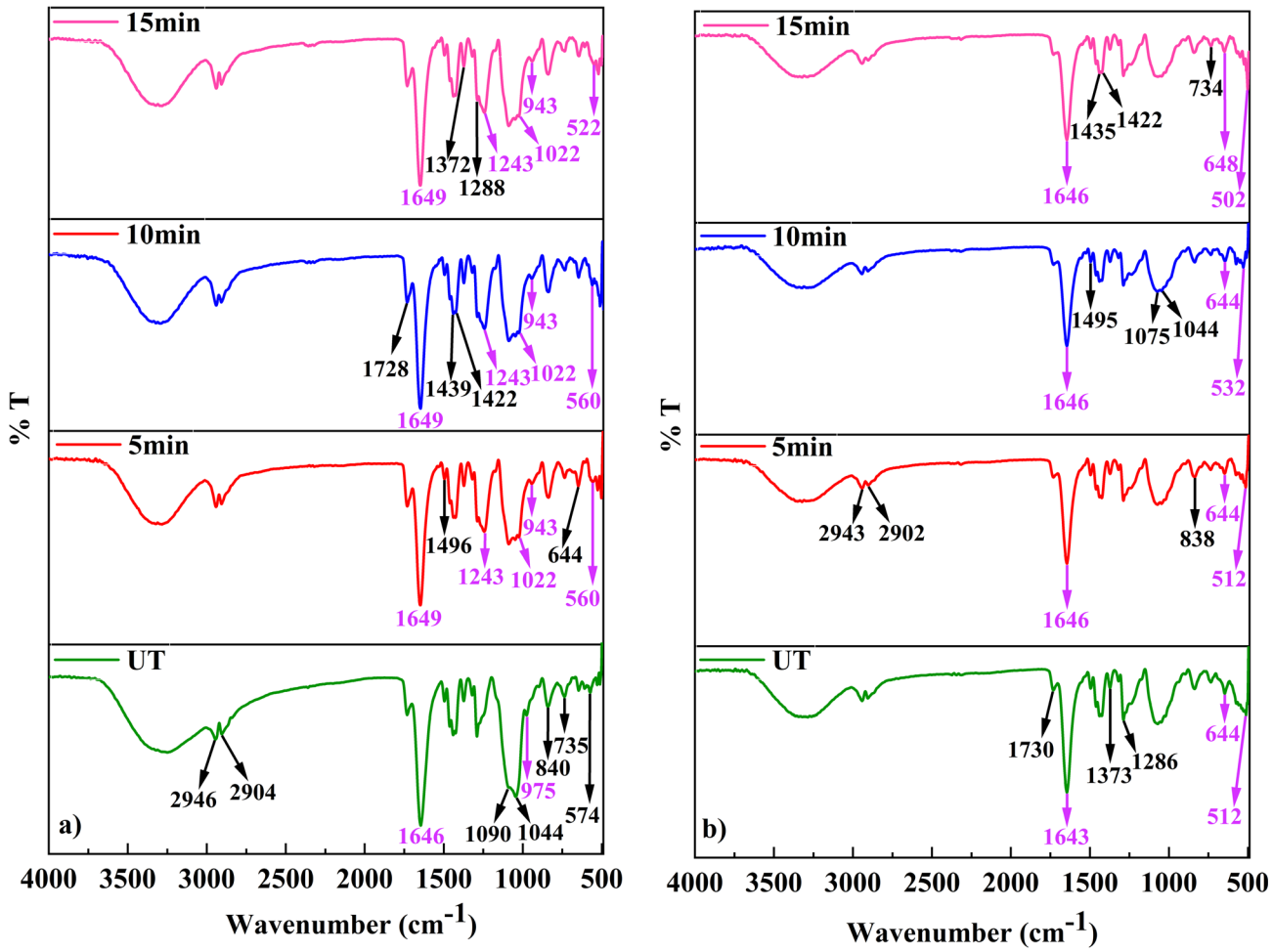

Fig. 5 FTIR analysis of (a) PVA/PVP/$CuSO_4$ and (b) PVA/PVP/$FeSO_4$ polymer films.

groups from the PVP component.[30] The C–O stretching vibration of PVA is observed at 1044 cm^{-1} in both films.[31] C–C stretching vibrations within the PVA–PVP polymer matrix are evident at the peaks 1090 and 840 cm^{-1} for $CuSO_4$ and 1075 and 838 cm^{-1} for $FeSO_4$, respectively.[30] The peak at 975 cm^{-1}, observed only in $CuSO_4$-based films, corresponds to C–H bending in PVA.[32] The peak at 735 cm^{-1} ($CuSO_4$) and 734 cm^{-1} ($FeSO_4$) represents the =C–H wagging vibrations in PVP. A distinct peak at 644 cm^{-1} is attributed to SO_4^{2-} bending,[33] which also overlaps with N–C=O deformation modes in PVP.[34] Additionally, peaks within the 500–600 cm^{-1} range represent the Cu–O ($CuSO_4$) and Fe–O ($FeSO_4$) stretching vibrational modes, confirming the incorporation of metal sulfates into the polymer matrix.[35,36] Plasma treatment resulted in spectral shifts and the appearance of new functional features. In the $CuSO_4$ based films, the peak at 1646 cm^{-1} shifted to 1649 cm^{-1}, and the band at 975 cm^{-1} shifted to 943 cm^{-1}, indicating alteration in the bonding environment and crosslinking. Furthermore, the new bands appeared at 1243 and 1022 cm^{-1}, attributed to C–O–C stretching vibrations contributes from the PVA/PVP blends[37,38] and potential plasma-induced crosslinking.[39] In the $FeSO_4$ films, the peak at 1643 cm^{-1} shifted to 1646 cm^{-1}, while the sulfate-related band at 644 cm^{-1} shifted slightly to 648 cm^{-1}, indicating slight modifications in the bonding environment, possibly resulting from crosslinking or surface oxidation effects due to plasma exposure.

3.5. XPS analysis

The effect of atmospheric DBD plasma treatment on the surface chemical composition of the polymer films was systematically investigated using XPS. The survey spectra and corresponding deconvoluted peaks provided insight into the elemental composition and binding environments of the major constituents and its corresponding images are given in the Fig. S2(a–d) and 6(a–h). In the case of PVA/PVP/$CuSO_4$ films, the primary

Table 1 Chemical composition of untreated and plasma-treated polymer films

	Atomic%				
Sample code	C 1s	O 1s	N 1s	Cu 2p/Fe 2p	S 2p
UT PVA/PVP/$CuSO_4$	73.44	23.01	1.54	1.89	0.12
PT15 PVA/PVP/$CuSO_4$	45.98	48.92	1.96	3.03	0.11
UT PVA/PVP/$FeSO_4$	70.90	24.72	3.90	0.38	0.10
PT15 PVA/PVP/$FeSO_4$	65.34	29.10	4.18	1.25	0.13

peaks were identified at binding energies of 285.2 eV (C1s), 532.3 eV (O1s), 400.1 eV (N1s), 935.3 eV (Cu2p) and 169.2 eV (S2p). After plasma treatment, a significant reduction in surface carbon content was observed, with the C1s atomic percentage decreasing from 73.44% to 45.98%, along with a notable increase in oxygen content from 23.01% to 48.92%. Similarly, for the PVA/PVP/$FeSO_4$ films, the detected peaks correspond to 285.4 eV (C1s), 532.3 eV (O1s), 400.1 eV (N1s), 711.9 eV (Fe2p),

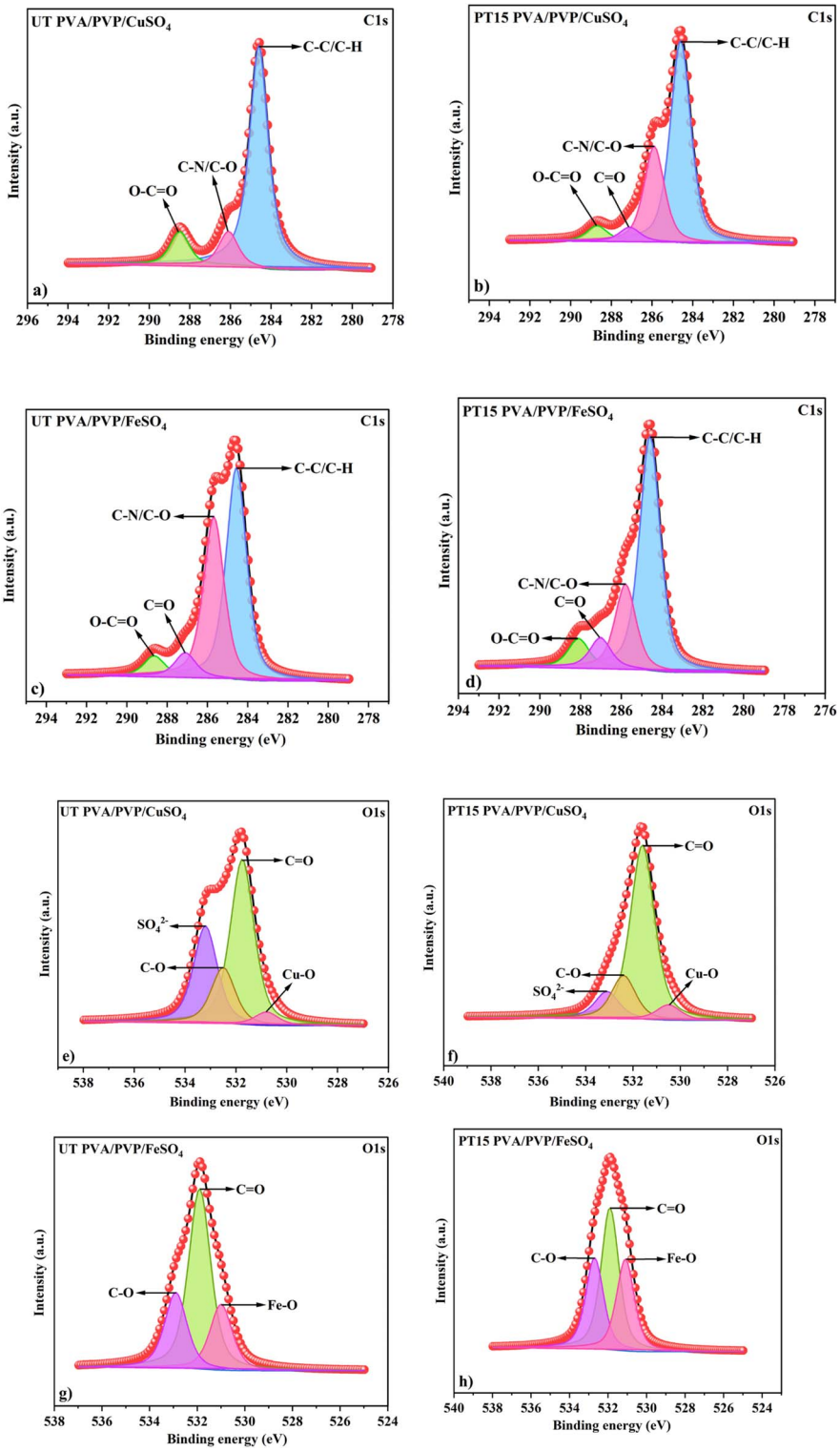

Fig. 6 Deconvoluted peaks of (a) C1s UT PVA/PVP/$CuSO_4$ (b) C1s PT15 PVA/PVP/$CuSO_4$ (c) C1s UT PVA/PVP/$FeSO_4$ (d) C1s PT15 PVA/PVP/$FeSO_4$ (e) O1s UT PVA/PVP/$CuSO_4$ (f) O1s PT15 PVA/PVP/$CuSO_4$ (g) O1s UT PVA/PVP/$FeSO_4$ (h) O1s PT15 PVA/PVP/$FeSO_4$.

and 169.2 eV (S2p), respectively. After plasma exposure, the carbon content decreased moderately from 70.90% to 65.34%, while the oxygen percentage increased from 24.72% to 29.10%, indicating enhanced surface oxidation and incorporation of oxygen-containing functional groups. The chemical composition of the untreated and plasma-treated polymer films is given in the Table 1.

The deconvoluted C1s and O1s spectra of the polymer films are presented in Fig. 6(a–h). To mitigate surface charging effects and ensure precise binding energy calibration, the C1s peak at 284.6 eV was used as a reference for all spectra. In Fig. 6a, the C1s spectrum of the untreated PVA/PVP/$CuSO_4$ film displays three distinct components. The peak at 284.6 eV is assigned to aliphatic hydrocarbons (C–C/C–H) originating from both PVA and PVP. The component at 286.1 eV corresponds to overlapping C–N and C–O groups present in the polymer matrix, while the peak at 288.6 eV is attributed to carboxyl functionalities (O–C═O) primarily from PVA. After plasma treatment (Fig. 6b), a new peak appears at 287.1 eV, indicating the formation of carbonyl groups (C═O) within the PVA and PVP structures. Additionally, the C–N/C–O peak undergoes a slight shift from 286.1 eV to 285.9 eV, suggesting subtle alterations in the local chemical environment due to plasma exposure. In the case of the untreated PVA/PVP/$FeSO_4$ film (Fig. 6c), the C1s spectrum is deconvoluted into four components located at 284.6, 285.7, 287.1 and 288.6 eV, corresponding to hydrocarbon (C–C/C–H), C–N/C–O, C═O, and O–C═O functional groups, respectively. After plasma treatment (Fig. 6d), the carboxyl peak at 288.6 eV shifts to 288.1 eV, indicating modification in the electronic structure of the oxygenated carbon species due to the rearrangement of functional groups.[40–44]

Fig. 6(e–h) presents the deconvoluted O1s spectra of both untreated and plasma-treated PVA/PVP/$CuSO_4$ and PVA/PVP/$FeSO_4$ films. For the untreated PVA/PVP/$CuSO_4$ film (Fig. 6e), four distinct peaks are identified at 530.8, 531.7, 532.5 and 533.2 eV, which are attributed to Cu–O bonds, carbonyl groups (C═O), C–O functionalities and sulfate species (SO_4^{2-}), respectively. These confirm the successful incorporation of $CuSO_4$ within the polymer matrix and the presence of oxygen-containing groups from PVA and PVP matrix. After plasma treatment (Fig. 6f), a noticeable shift in the Cu–O binding energy from 530.8 eV to 530.5 eV is observed, indicating modifications in the metal–oxygen coordination environment due to the electronic redistribution at the interface. In the case of the untreated PVA/PVP/$FeSO_4$ film (Fig. 6g), the O1s spectrum shows three peaks located at 531.0, 531.9 and 532.9 eV, corresponding to Fe–O bonds, carbonyl (C═O) and C–O groups of the PVA/PVP matrix, respectively. After plasma exposure (Fig. 6h), a minor shift in the C–O peak from 532.9 eV to 532.7 eV is observed, which reflects slight changes in the chemical bonding and surface oxidation states of the polymeric components.[45–49] XPS analysis confirms that plasma treatment induces significant chemical modifications, including the incorporation of additional oxygen-containing functional groups and changes in metal–oxygen interactions. These alterations indicate chemical restructuring within the polymer

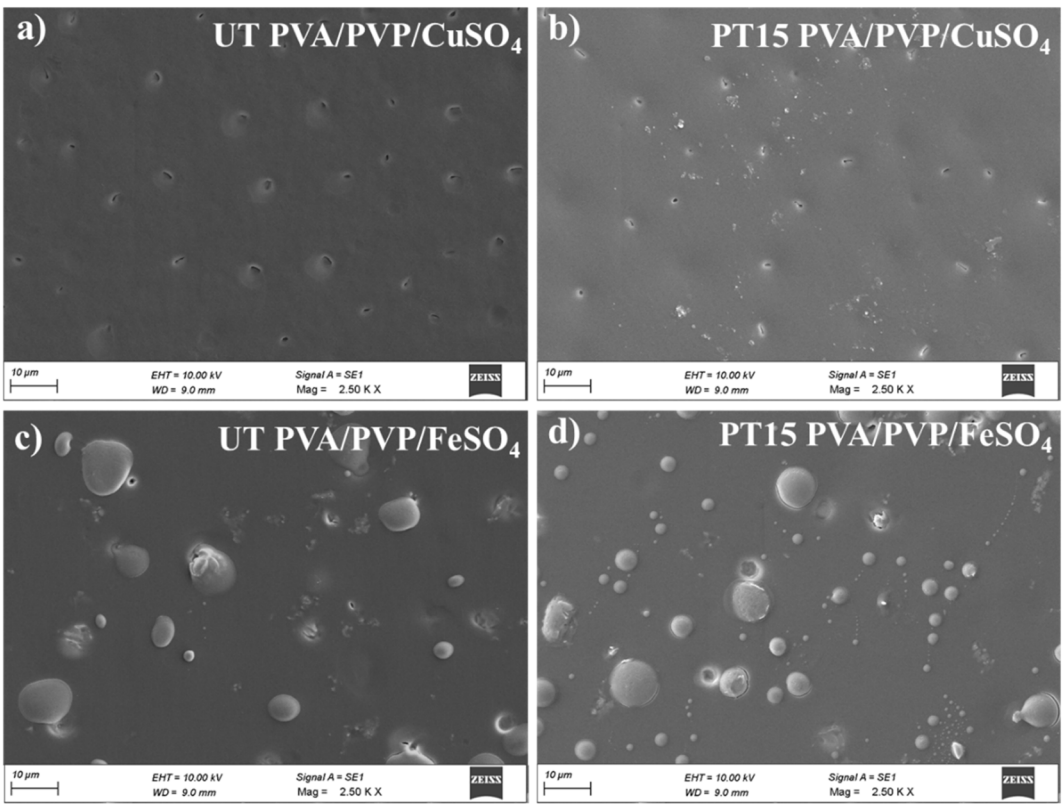

Fig. 7 SEM analysis of PVA/PVP/$CuSO_4$ and PVA/PVP/$FeSO_4$ polymer films.

matrix, which can be attributed to plasma-induced crosslinking.[50,51]

3.6. SEM analysis

The surface morphology of the synthesized PVA/PVP/$CuSO_4$ and PVA/PVP/$FeSO_4$ films before and after plasma treatment was investigated using SEM analysis as shown in the Fig. 7(a–d).

The untreated PVA/PVP/$CuSO_4$ films (Fig. 7a) displayed a smooth and uniform surface with sparsely distributed micropores, suggesting a relatively homogeneous dispersion of $CuSO_4$ within the polymer matrix and minimal surface aggregation. After plasma treatment (Fig. 7b), the surface exhibited noticeable morphological changes, characterized by increased surface roughness and the formation of fine surface pores. These morphological changes are attributed to the physical etching and activation caused by plasma exposure, which modifies only the top surface layer of the film without altering its internal composition. In the case of the untreated PVA/PVP/$FeSO_4$ film (Fig. 7c), the surface displayed numerous distinct spherical structures, corresponding to the $FeSO_4$ particles embedded within the polymer matrix. Upon plasma treatment (Fig. 7d), a reduction in size and density of these aggregates was observed, indicating surface-level rearrangements as a result of plasma exposure. The SEM analysis demonstrates that DBD argon plasma treatment significantly alters the surface morphology of both polymer films by increasing surface roughness. These changes were further quantified through AFM analysis to determine the average surface roughness values.

3.7. AFM analysis

AFM analysis was employed to investigate the surface topography and average surface roughness (R_a) of the synthesized PVA/PVP/$CuSO_4$ and PVA/PVP/$FeSO_4$ films before and after plasma treatment as shown in Fig. 8(a–d).

The untreated PVA/PVP/$CuSO_4$ film (Fig. 8a) exhibited a relatively smooth surface with a low R_a of 0.83 ± 0.15 nm, indicating minimal surface irregularities and a uniform

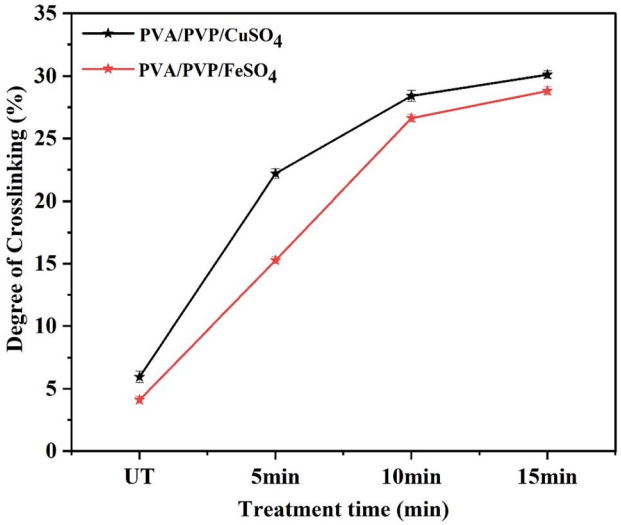

Fig. 9 Degree of crosslinking of PVA/PVP/$CuSO_4$ and PVA/PVP/$FeSO_4$ polymer films.

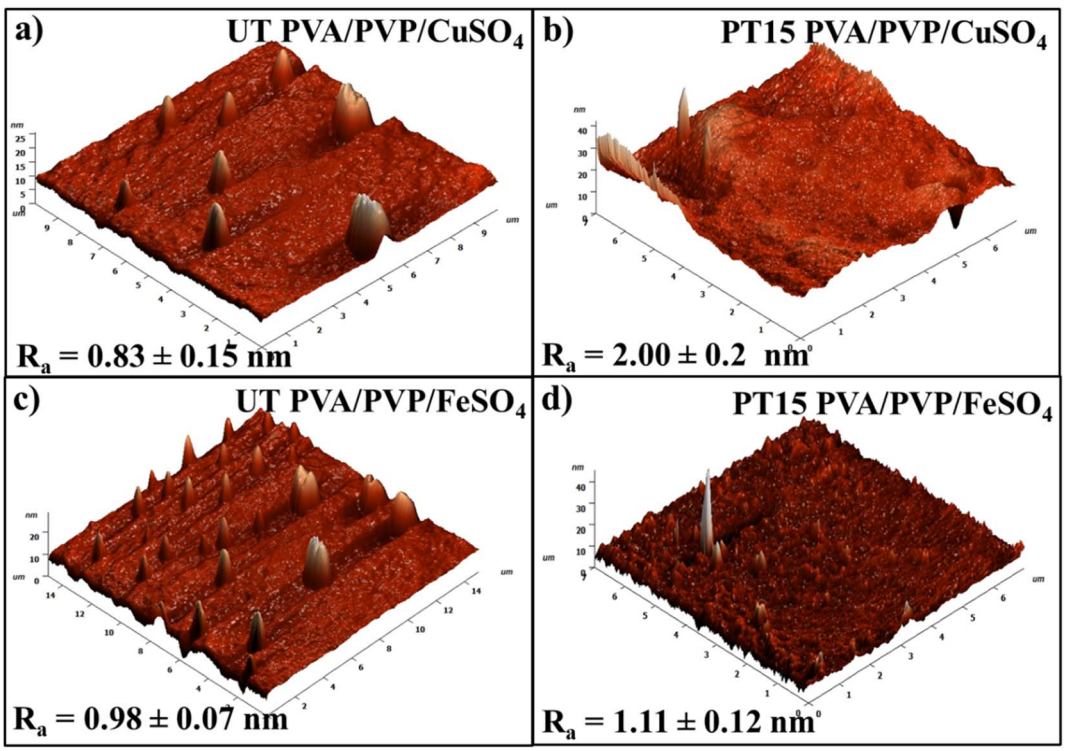

Fig. 8 AFM analysis of PVA/PVP/$CuSO_4$ and PVA/PVP/$FeSO_4$ polymer films.

dispersion of $CuSO_4$ within the polymer matrix. After plasma treatment (Fig. 8b), a significant increase in surface roughness was observed, with an R_a value of 2.00 ± 0.2 nm. The increase in roughness can be attributed to surface activation and etching effects induced by high-energy argon species, which result in the formation of nano-scale surface changes and an overall rougher texture. Similarly, the untreated PVA/PVP/$FeSO_4$ film (Fig. 8c) presented a moderate rough surface with R_a of 0.98 ± 0.07 nm, attributed to the presence of $FeSO_4$ aggregates. After plasma exposure (Fig. 8d), the surface became further textured with an R_a increased to 1.11 ± 0.12 nm. The topographic image revealed a more granular appearance, indicating the redistribution of $FeSO_4$ aggregates due to the plasma-induced physical interactions at the film surface. The observed increases in

Table 2 Mechanical properties of untreated and plasma-treated polymer films

Polymer films	Tensile strength (MPa)	Elongation at break (%)
UT PVA/PVP/$CuSO_4$	15.08 ± 1.13	251.50 ± 4.76
PT15 PVA/PVP/$CuSO_4$	25.93 ± 3.48	235.73 ± 4.30
UT PVA/PVP/$FeSO_4$	15.78 ± 3.15	262.80 ± 4.85
PT15 PVA/PVP/$FeSO_4$	21.70 ± 3.93	195.80 ± 5.93

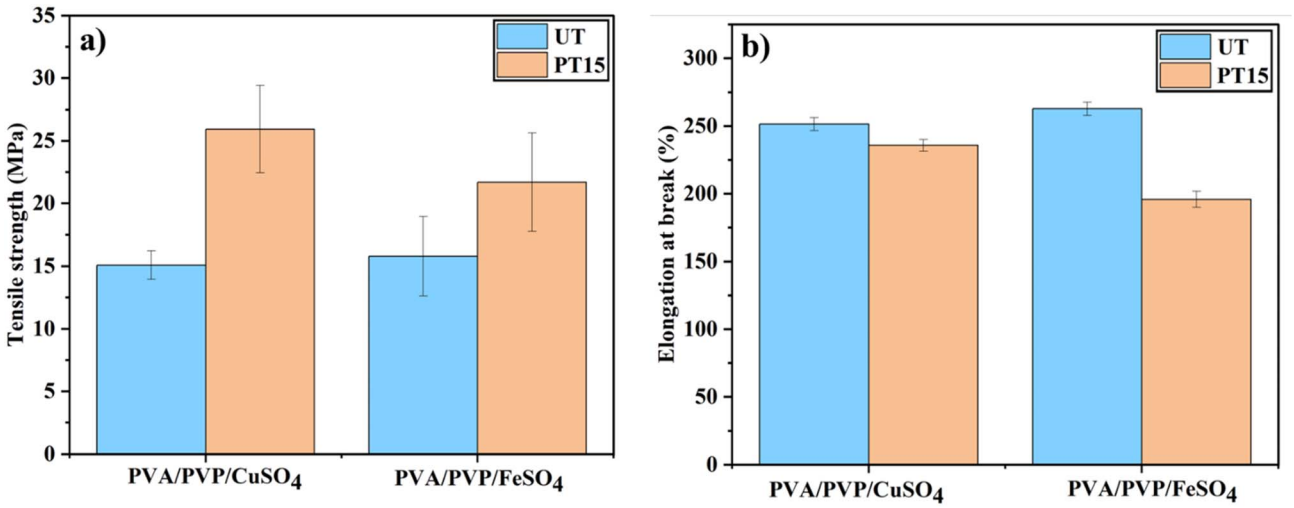

Fig. 10 (a) Tensile strength and (b) elongation at break of PVA/PVP/$CuSO_4$ and PVA/PVP/$FeSO_4$ polymer films.

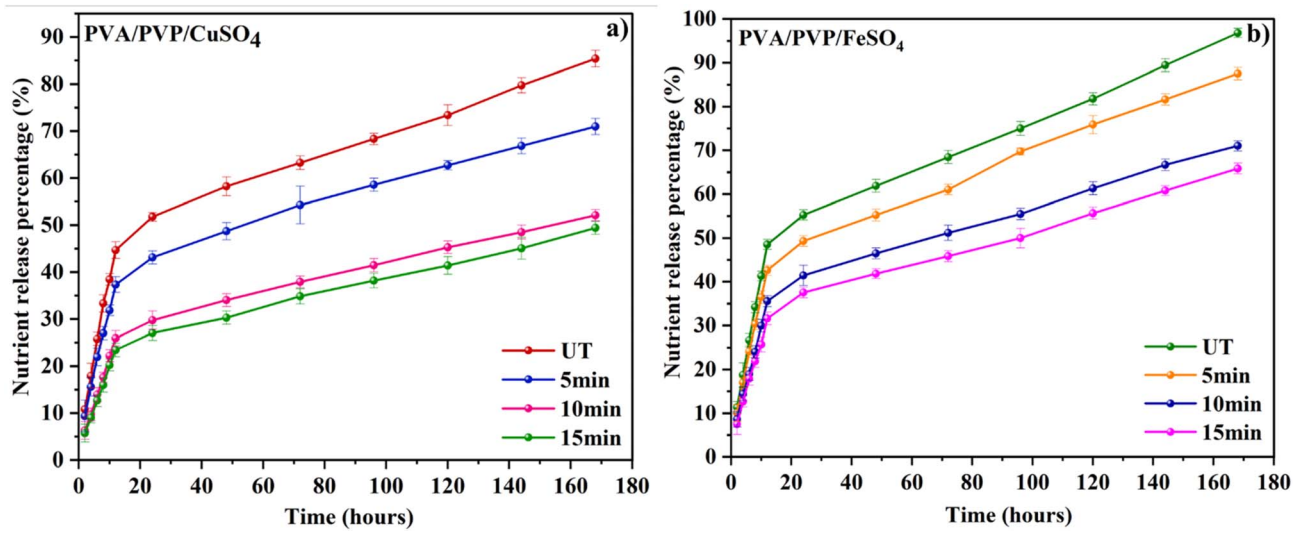

Fig. 11 *In vitro* nutrient release test of (a) PVA/PVP/$CuSO_4$ and (b) PVA/PVP/$FeSO_4$ polymer films.

Table 3 Correlation coefficient (R^2) value of nutrient release kinetic models for untreated and plasma-treated polymer films

Sample code	Zero order	First order	Higuchi	Korsmeyer–Peppas
UT PVA/PVP/$CuSO_4$	0.834	0.951	0.927	0.904
PT15 PVA/PVP/$CuSO_4$	0.877	0.924	0.952	0.929
UT PVA/PVP/$FeSO_4$	0.859	0.919	0.940	0.913
PT15 PVA/PVP/$FeSO_4$	0.872	0.939	0.949	0.926

surface roughness for both PVA/PVP/$CuSO_4$ and PVA/PVP/$FeSO_4$ films demonstrate the effectiveness of DBD argon plasma in modifying the outermost layer of the polymer films.

3.8. Degree of crosslinking

Fig. 9 illustrates the degree of crosslinking for all the polymer film samples. The untreated films exhibited a relatively low degree of crosslinking, whereas the plasma-treated films showed a significant increase in crosslinking with longer treatment durations. The degree of crosslinking for untreated PVA/PVP/$CuSO_4$ films was calculated to be 5.94 ± 0.46% which increased to 30.50 ± 0.29% after 15 minutes of plasma exposure. A similar trend was observed in the PVA/PVP/$FeSO_4$ films, where the crosslinking degree increases from 4.11 ± 0.30% to 28.81 ± 0.32% over the same treatment duration. This enhancement in crosslinking is attributed to plasma-induced surface activation, which promotes the formation of additional intermolecular interactions and crosslinking sites within the polymer matrix. The resulting enhancement in crosslinked network density strengthens the structural integrity of the films and plays a crucial role in maintaining a sustained and controlled release of the nutrients.

3.9. Mechanical properties

The mechanical behavior of untreated (UT) and plasma-treated (PT15) PVA/PVP films embedded with $CuSO_4$ and $FeSO_4$ was evaluated in terms of tensile strength and elongation at break as shown in the Table 2, Fig. 10a and b.

For the PVA/PVP/$CuSO_4$ films, the untreated sample exhibited a tensile strength of 15.08 ± 1.13 MPa and an elongation at break of 251.50 ± 4.76%. After 15 minutes of plasma treatment, the tensile strength significantly increased to 25.93 ± 3.48 MPa, while the elongation slightly decreased to 235.73 ± 4.30%. Similarly, for PVA/PVP/$FeSO_4$ films, the tensile strength increased from 15.78 ± 3.15 MPa (UT) to 21.70 ± 3.93 MPa (PT15), whereas elongation decreased from 262.80 ± 4.85% to 195.80 ± 5.93%. The observed enhancement in tensile strength after plasma treatment can be attributed to plasma-induced crosslinking and chemical modifications that reinforce the polymer network and increase film rigidity. Conversely, the reduction in elongation at break is likely due to the compact rearrangement of polymer chains and reduced chain mobility caused by energetic plasma exposure. Although plasma treatment caused a moderate reduction in elongation at break, the values remained relatively high, indicating that the films retain substantial flexibility. These findings are in good agreement with previous reports.[52,53]

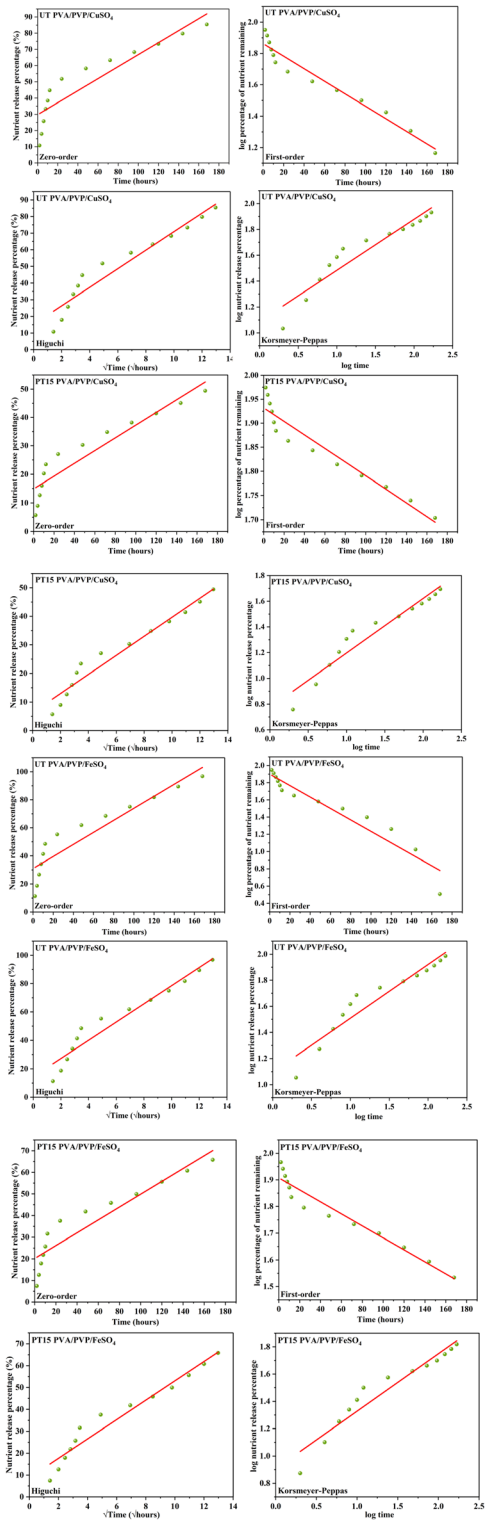

Fig. 12 Various nutrient release kinetic models of untreated and plasma-treated PVA/PVP/$CuSO_4$ and PVA/PVP/$FeSO_4$ polymer films.

3.10. Nutrient release test

The *in vitro* nutrient release behavior of the synthesized polymer films was evaluated to assess their suitability for controlled nutrient delivery in agricultural applications. Fig. 11a and b illustrate the cumulative nutrient release profiles of untreated and plasma-treated PVA/PVP/$CuSO_4$ and PVA/PVP/$FeSO_4$ films over a period of 168 hours. For the PVA/PVP/$CuSO_4$ films, the untreated sample exhibited a higher nutrient release rate of 85.4 ± 1.8% at 168 hours. Plasma-treated films demonstrated a gradual reduction in release rates with increasing treatment duration. The 5 min treated film released about 70.9 ± 1.7%, while 10 min and 15 min treated films released 52.1 ± 1.2% and 49.4 ± 1.4% respectively. A similar trend was observed in PVA/PVP/$FeSO_4$ films as shown in Fig. 11b. The untreated film exhibited a slightly higher release rate of 96.8 ± 1.1% compared to its $CuSO_4$ counterpart. The release rate decreased to 87.5 ± 1.4%, 71.0 ± 1.2% and 65.8 ± 1.3% for 5, 10 and 15 min plasma-treated films. These results indicate that DBD argon plasma treatment significantly influences the nutrient release behavior of the polymer films. The observed reduction in release rate is primarily attributed to the plasma-induced surface crosslinking and etching effects. Surface crosslinking reduces the polymer chain mobility and hinders nutrient diffusion, while plasma-induced etching and functionalization modify the surface chemistry, forming a semi-permeable barrier that controls nutrient passage. Also, plasma-induced structural rearrangements contribute to the formation of a more compact surface layer, which limits the water uptake and slows the release process. Although an increase in surface hydrophilicity was observed after plasma treatment, the dominant effect of crosslinking and structural modification resulted in slower nutrient release kinetics. Such controlled and sustained release profiles are highly beneficial in agricultural systems, as they reduce nutrient loss and enhance nutrient use efficiency over time.

3.11. Nutrient release kinetics

The nutrient release profiles of the synthesized PVA/PVP/$CuSO_4$ and PVA/PVP/$FeSO_4$ films were further evaluated through kinetic models to elucidate the underlying release mechanisms. The experimental data were fitted to four commonly used models such as zero-order, first-order, Higuchi and Korsmeyer–Peppas models, and the corresponding correlation coefficients (R^2) are presented in the Table 3.

For the untreated PVA/PVP/$CuSO_4$ film, the first-order model exhibited the best fit (R^2 = 0.951), followed by the Higuchi model (R^2 = 0.927), indicating that the release was primarily governed by a concentration gradient with an additional contribution from diffusion. In contrast, the plasma-treated PVA/PVP/$CuSO_4$ films (15 min treatment) showed the highest correlation with the Higuchi model (R^2 = 0.952), signifying a shift toward diffusion-dominated release, likely due to surface

Table 4 Comparison of various materials and fertilizers with release behavior reported in the literatures

Material	Fertilizer/ micronutrient	Crosslinking/treatment method	Release%	Release time	Ref.
Starch carbamate/sodium alginate hydrogel	Urea	Crosslinked *via* cationic ion interaction, forming a denser hydrogel network to slow urea diffusion	90.2%	16 hours	54
Corn starch/PVA/alkali lignin	Urea	Chemical crosslinking between alkali lignin and PVA/starch molecular chains restricted nutrient mobility	64%	120 minutes	55
Zn-GO pellets and Cu–GO pellets	$ZnSO_4$, $CuSO_4$	Micronutrients adsorbed onto graphene oxide nanosheets and compacted into pellets; strong ion–GO interactions slowed release	~55%	72 hours	56
Enteromorpha polysaccharide/Konjac glucomannan mulch/biochar films	Urea	Urea-loaded biochar incorporated into polysaccharide/Konjac composite films reduced rapid release	76.9%	20 hours	57
Biochar–NPK pellets coated with kaolinite/PVA/starch	N, P, K	Biochar–NPK fertilizer pellets were coated with a crosslinked PVA/starch/kaolinite solution (crosslinking *via* KPS, glycerin as plasticizer) using a simple coating machine; the coating layer acted as a barrier to slow nutrient release	~75% (N, P), ~80% (K)	18 hours	58
PVA/PVP/$CuSO_4$	$CuSO_4$	Non-thermal plasma treatment induced surface crosslinking and structural rearrangement, restricting Cu^{2+} diffusion within the polymer matrix	49.4 ± 1.4%	168 hours	This work
PVA/PVP/$FeSO_4$	$FeSO_4$	Non-thermal plasma treatment induced surface crosslinking and structural rearrangement, restricting Fe^{2+} diffusion within the polymer matrix	65.8 ± 1.3%	168 hours	This work

modifications and possible crosslinking induced by plasma exposure. In contrast, PVA/PVP/$FeSO_4$ film exhibited a distinct behavior. The untreated films followed the Higuchi model ($R^2 = 0.940$), indicating that Fe^{2+} release was primarily controlled by Fickian diffusion from the outset. After 15 minutes of plasma treatment, the fundamental release mechanism remained unchanged, with the Higuchi model remained the best fit ($R^2 = 0.949$), reinforcing the diffusion-controlled nature of release. But, a slight reduction in the overall release rate was observed compared to untreated films, which can be attributed to the structural rearrangements and surface compaction caused by plasma exposure, which restricts the nutrient mobility within the matrix without altering the diffusion-controlled nature of the release. Therefore, while the Cu^{2+} system displayed a clear shift from concentration-gradient-driven release to diffusion-controlled release due to plasma-induced structural modifications, the Fe^{2+} system maintained its diffusion-dominated behavior with minor suppression in ion mobility. These observations highlight that the effect of plasma treatment on release kinetics is ion-specific and depends strongly on the interaction between the metal ions and the polymer matrix Fig. 12.

The Korsmeyer–Peppas model also demonstrated good correlation with the R^2 values ranging between 0.904 and 0.929. This suggests that the nutrient release may not follow a purely Fickian mechanism but rather involves anomalous transport processes that combine diffusion with polymer matrix relaxation, particularly in the plasma-treated films. Table 4 compares the nutrient release behavior of different materials reported in previous studies.

4 Conclusion

In this study, PVA/PVP/$CuSO_4$ and PVA/PVP/$FeSO_4$ composite films were prepared using the solution-casting method and subsequently modified using non-thermal DBD plasma. To evaluate the effects of plasma treatment on the structural and surface properties of the films, characterization techniques such as FTIR, SEM, AFM and XPS were employed. These analyses confirmed significant enhancements in surface characteristics after plasma exposure, including increased roughness, improved hydrophilicity and the introduction of new oxygen-containing functional groups on the surface of the polymer films. Importantly, plasma treatment also facilitated surface-level crosslinking between polymer chains, leading to a denser network structure. This plasma-induced crosslinking increased the tensile strength of both polymer films and reduced the diffusivity of embedded ions, thereby modulating the nutrient release behavior of the films. *In vitro* nutrient release studies demonstrated a notable decrease in the release rate of Cu^{2+} ions from the PVA/PVP/$CuSO_4$ films, dropping from $85.4 \pm 1.8\%$ in the untreated films to $49.4 \pm 1.4\%$ after plasma modification. This indicates a more sustained and controlled release profile, attributed to the plasma-induced surface modifications that likely altered diffusion pathways and film permeability. Additionally, kinetic modeling of the release data after plasma treatment revealed a better fit to the Higuchi model, suggesting that the nutrient release is predominantly governed by a diffusion-controlled mechanism. The combined effects of surface oxidation, morphological changes and crosslinking contributed to a more sustained and controlled release profile. These findings highlight the potential of plasma-treated polymeric systems as advanced platforms for controlled micronutrient delivery in agricultural applications.

While numerous studies have focused on bio-based, biodegradable polymer films for controlled nutrient delivery for sustainable agricultural applications,[59,60] this study employs PVA/PVP films due to their well-established film-forming properties and suitability for plasma surface modification. This work specifically examines how plasma treatment affects micronutrient release, providing a basis for future exploration of fully biodegradable polymer systems using plasma-assisted strategies. Although promising results are reported here, future research could examine soil interactions and plant uptake to validate the agronomic relevance of these films.

Author contributions

Nandhu Varshini Gnanasekar: methodology, investigation, formal analysis, conceptualization, writing – original draft. Shanmugavelayutham Gurusamy: supervision, resources, writing – review and editing.

Conflicts of interest

The authors declare no conflicts of interest.

Data availability

All data supporting this article are presented within the paper, and all information sourced from the literature has been properly cited.

Supplementary information is available. See DOI: **https://doi.org/10.1039/d5fb00462d**.

Acknowledgements

One of the author Nandhu Varshini Gnanasekar thank Department of Science and Technology, Ministry of Science and Technology, India for the financial support under DST-INSPIRE Fellowship [DST/INSPIRE Fellowship/2022/IF220156]. The authors thank Rashtriya Uchchatar Shiksha Abhiyan (RUSA) for providing the instrumental facility.

References

1 Y. M. Adal and K. S. Mulat, Micronutrient Limitations in Crop Production and Strategies for Improvement: A Review, 2024, DOI: **10.21203/rs.3.rs-3931101/v1**.

2 P. B. Linares, L. A. Castillo and S. E. Barbosa, Micronutrients release from active polyethylene films under mulched conditions, *Results Surf. Interf.*, 2025, **18**, 100419, DOI: **10.1016/j.rsurfi.2025.100419**.

3 D. K. Tripathi, S. Singh, S. Singh, S. Mishra, D. K. Chauhan and N. K. Dubey, Micronutrients and their diverse role in agricultural crops: advances and future prospective, *Acta Physiol. Plant.*, 2015, **37**(7), 139, DOI: **10.1007/s11738-015-1870-3**.

4 L. M. Shuman, *Micronutrient Fertilizers, Nutrient Use in Crop Production*, CRC Press, 1st edn, 2017, pp. 165–195, DOI: **10.1300/J144v01n02_07**.

5 C. G. Chiaregato, C. F. Souza and R. Faez, Plasticized poly(vinyl alcohol)/starch as a nutrient delivery system for macro and micronutrients, *ACS Agric. Sci. Technol.*, 2023, **3**(4), 322–333, DOI: **10.1021/acsagscitech.2c00313**.

6 P. B. Linares, L. A. Castillo and S. E. Barbosa, Controlled release of micronutrients from surface-modified polymer films for agricultural applications, *J. Mater. Sci.*, 2021, **56**(15), 9134–9156, DOI: **10.1007/s10853-020-05755-4**.

7 H. M. Zidan, E. M. Abdelrazek, A. M. Abdelghany and A. E. Tarabiah, Characterization and some physical studies of PVA/PVP filled with MWCNTs, *J. Mater. Res. Technol.*, 2019, **8**(1), 904–913, DOI: **10.1016/j.jmrt.2018.04.023**.

8 S. A. Soud, B. A. Hasoon, A. I. Abdulwahab, N. N. Hussein and R. K. Maeh, Synthesis and characterization of plant extracts loaded PVA/PVP blend films and evaluate their biological activities, *EurAsian J. BioSci.*, 2020, **14**(2), 2921–2931.

9 P. Wen, T. G. Hu, Y. Wen, K. E. Li, W. P. Qiu, Z. L. He, H. Wang and H. Wu, Development of Nervilia fordii extract-loaded electrospun pva/pvp nanocomposite for antioxidant packaging, *Foods*, 2021, **10**(8), 1728, DOI: **10.3390/foods10081728**.

10 S. F. El-Gioushy, R. Sami, A. A. Al-Mushhin, H. M. Abou El-Ghit, M. S. Gawish, K. A. Ismail and R. M. Zewail, Foliar application of ZnSO4 and CuSO4 affects the growth, productivity, and fruit quality of Washington Navel orange trees (Citrus sinensis L.) Osbeck, *Horticulturae*, 2021, **7**(8), 233, DOI: **10.3390/horticulturae7080233**.

11 A. Saleem, A. Zulfiqar, B. Ali, M. A. Naseeb, A. S. Almasaudi and S. Harakeh, Iron sulfate (FeSO4) improved physiological attributes and antioxidant capacity by reducing oxidative stress of Oryza sativa L. cultivars in alkaline soil, *Sustainability*, 2022, **14**(24), 16845, DOI: **10.3390/su142416845**.

12 N. V. Gnanasekar and S. Gurusamy, Impact of Atmospheric Pressure Nonthermal Plasma on Curcumin-Loaded Polyvinyl Alcohol/Chitosan Polymer Films for Controlled Drug Release Application, *IEEE Trans. Plasma Sci.*, 2024, **52**(12), 5538–5560, DOI: **10.1109/TPS.2024.3513560**.

13 N. V. Gnanasekar and S. Gurusamy, Study on antibacterial efficiency of ZnO functionalized plasma-treated PMMA and PS polymer films for Bio-medical applications, *Vacuum*, 2025, **240**, 114469, DOI: **10.1016/j.vacuum.2025.114469**.

14 T. Felix, J. S. Trigueiro, N. Bundaleski, O. M. Teodoro, S. Sério and N. A. Debacher, Functionalization of polymer surfaces by medium frequency non-thermal plasma, *Appl. Surf. Sci.*, 2018, **428**, 730–738, DOI: **10.1016/j.apsusc.2017.09.147**.

15 T. Jacobs, R. Morent, N. De Geyter, P. Dubruel and C. Leys, Plasma surface modification of biomedical polymers: influence on cell-material interaction, *Plasma Chem. Plasma Process.*, 2012, **32**(5), 1039–1073, DOI: **10.1007/s11090-012-9394-8**.

16 ASTM D882-01, Standard Test Method for Tensile Properties of Thin Plastic, *Sheeting*, ASTM International, West Conshohocken, PA, USA, 2001.

17 G. Yadav, M. Bansal, N. Thakur, S. Khare and P. Khare, Multilayer tablets and their drug release kinetic models for oral controlled drug delivery system, *ME J Sci Res.*, 2013, **16**, 782–795, DOI: **10.5829/idosi.mejsr.2013.16.06.75176**.

18 E. Vassallo, M. Pedroni, M. Aloisio, S. M. Pietralunga, R. Donnini, F. Saitta and D. Fessas, Plasma treatment of different biodegradable polymers: a method to enhance wettability and adhesion properties for use in industrial packaging, *Plasma*, 2024, **7**(1), 91–105, DOI: **10.3390/plasma7010007**.

19 G. Dalei, S. Das, S. R. Jena, J. Nayak, L. Samanta and S. P. Das, Improved chemosensitization activity of carboxymethyl chitosan/PVA hydrogels by plasma surface modification, *J. Polym. Environ.*, 2021, **29**(5), 1663–1679, DOI: **10.1007/s10924-020-02007-z**.

20 N. M. Deghiedy and S. M. El-Sayed, Evaluation of the structural and optical characters of PVA/PVP blended films, *Opt. Mater.*, 2020, **100**, 109667, DOI: **10.1016/j.optmat.2020.109667**.

21 B. Xue, J. Zhang and T. Zhou, Moving-window two-dimensional correlation infrared spectroscopic study on the dissolution process of poly (vinyl alcohol), *Anal. Bioanal. Chem.*, 2015, **407**(29), 8765–8771, DOI: **10.1007/s00216-015-9035-1**.

22 H. M. Gayitri, M. Q. Al-Gunaid and J. R. Kumar, Investigation on optical, structural and electrochemical properties of hybrid PVA/ZnWMoO7 nanocomposite film for optoelectronics and super capacitor applications, *Polym. Bull.*, 2023, **80**(8), 8665–8683, DOI: **10.1007/s00289-022-04458-x**.

23 D. Mondal, M. M. Mollick, B. Bhowmick, D. Maity, M. K. Bain, D. Rana, A. Mukhopadhyay, K. Dana and D. Chattopadhyay, Effect of poly (vinyl pyrrolidone) on the morphology and physical properties of poly (vinyl alcohol)/sodium montmorillonite nanocomposite films, *Prog. Nat. Sci.:Mater. Int.*, 2013, **23**(6), 579–587, DOI: **10.1016/j.pnsc.2013.11.009**.

24 A. A. Ben, N. Bouchikhi and M. Benhaliliba, A study of thermal stability, vibrational spectroscopy, electric response and linear and nonlinear optical properties of pure PVP polymer for solar cell and NLO devices, *Opt. Quantum Electron.*, 2023, **55**(1), 66, DOI: **10.1007/s11082-022-04346-8**.

25 M. C. Popescu, C. Vasile and B. C. Simionescu, 2D IR DICHROISM SPECTRA OF POLY (VINYL ALCOHOL), *Rev. Roum. Chim.*, 2012, **57**(7–8), 659–664.

26 A. L. Soares, J. D. de Moraes, M. A. D'Ávila, F. K. Andrade and R. S. Vieira, Production and characterization of membranes containing PCL and PVP obtained by simultaneous and

blends electrospinning, *International Journal of Advances in Medical Biotechnology*, 2020, **3**(1), 16–22.

27 S. Muhamad, H. Mohamed Kamari, N. M. Al-Hada, C. A. Abdullah and N. N. Nidzam, Fabrication of binary (ZnO) x (TiO2) 1− x nanoparticles *via* thermal treatment route and evaluating the impact of various molar concentrations on the structure and optical behaviors, *Appl. Phys. A*, 2020, **126**(8), 587, DOI: 10.1007/s00339-020-03701-4.

28 S. Choudhary, Characterization of amorphous silica nanofiller effect on the structural, morphological, optical, thermal, dielectric and electrical properties of PVA–PVP blend based polymer nanocomposites for their flexible nanodielectric applications, *J. Mater. Sci.: Mater. Electron.*, 2018, **29**(12), 10517–10534, DOI: 10.1007/s10854-018-9116-y.

29 R. Ramadan and A. M. Ismail, Structural and physical comparison between CS/PVP blend and CS/PVP/Sr-Hexaferrite nanocomposite films, *J. Inorg. Organomet. Polym. Mater.*, 2023, **33**(8), 2506–2516, DOI: 10.1007/s10904-023-02684-y.

30 S. Jha, V. Bhavsar, K. P. Sooraj, M. Ranjan and D. Tripathi, Investigation of the effect of in-situ grown PPy on low frequency dielectric properties and other properties of PVA-PVP blend film, *J. Adv. Dielectr.*, 2021, **11**(04), 2150020, DOI: 10.1142/S2010135X2150020X.

31 C. Salma and B. H. Rudramadevi, Spectroscopic properties of Ho 3: PVA/PVP blend polymer films, *J. Appl. Phys.*, 2020, **6**(12), 35–44, DOI: 10.9790/4861-1206023544.

32 M. Muthiah, G. Chellasamy, R. Natarajan, S. Subramanian and S. Chinnappa, Proton conducting polymer electrolytes based on PVdF-PVA with NH4NO3, *J. Polym. Eng.*, 2013, **33**(4), 315–322, DOI: 10.1515/polyeng-2012-0146.

33 R. L. Frost, A. López, R. Scholz, Y. Xi, A. J. da Silveira and R. M. Lima, Characterization of the sulphate mineral amarantite–Fe23+ (SO4) O· 7H2O using infrared, Raman spectroscopy and thermogravimetry, *Spectrochim. Acta, Part A*, 2013, **114**, 85–91, DOI: 10.1016/j.saa.2013.04.111.

34 S. Hamimed, N. E. Ammar, H. Slimi, N. Asses, A. H. Hamzaoui and A. Chatti, Innovative entrapped Yarrowia lipolytica within polyvinylpyrrolidone (PVP)/polyethylene glycol (PEG)/agar for improving olive mill wastewater bioremediation, *J. Cleaner Prod.*, 2024, **449**, 141828, DOI: 10.1016/j.jclepro.2024.141828.

35 A. Isiyaku, N. Y. Pindiga, U. A. Musa, S. M. Bappah, B. Muhammad, J. Joshua and M. B. Sulaiman, Synthesis, characterization and comparative antibacterial study of Copper II and Zinc II Vanillin-2-aminophenol Schiff base and their mixed ligand Complexes, *BIMA Journal Of Science And Technology*, 2024, **8**(3A), 282–289, DOI: 10.56892/bima.v8i3A.812.

36 S. Musić, S. Popović and S. Dalipi, Formation of oxide phases in the system Fe2O3-NiO, *J. Mater. Sci.*, 1993, **28**(7), 1793–1798, DOI: 10.1007/BF00595747.

37 P. Wen, T. G. Hu, Y. Wen, K. E. Li, W. P. Qiu, Z. L. He, H. Wang and H. Wu, Development of Nervilia fordii extract-loaded electrospun pva/pvp nanocomposite for antioxidant packaging, *Foods*, 2021, **10**(8), 1728, DOI: 10.3390/foods10081728.

38 P. Ramisetti, V. Maragani, S. K. Danikonda, B. Nampally and M. Katakam, Role of bimetallic (Ag-Cu) nanoparticles on the structural properties of PVA/PVP blend green nanocomposites, *J. Polymer Compos.*, 2022, **10**(11), 19, DOI: 10.37591/JoPC.

39 M. H. Abdel-Kader, A. A. Mohamed, J. Q. Almarashi and M. B. Mohamed, Investigating the tunable properties of double blended nanocomposite films exposed to direct Nd: YAG laser beam, *Opt. Mater.*, 2023, **142**, 114100, DOI: 10.1016/j.optmat.2023.114100.

40 M. Sun, Y. Wang, L. Yao, Y. Li, Y. Weng and D. Qiu, Fabrication and characterization of gelatin/polyvinyl alcohol composite scaffold, *Polymers*, 2022, **14**(7), 1400, DOI: 10.3390/polym14071400.

41 B. Sreedhar, M. Sairam, D. K. Chattopadhyay, P. S. Rathnam and D. M. Rao, Thermal, mechanical, and surface characterization of starch–poly (vinyl alcohol) blends and borax-crosslinked films, *J. Appl. Polym. Sci.*, 2005, **96**(4), 1313–1322, DOI: 10.1002/app.21439.

42 A. Bijanu, G. Rajak, R. Paulose, R. Arya, V. Agrawal, V. S. Gowri, M. A. Khan, S. T. Salammal and D. Mishra, Flexible, chemically bonded Bi-PVA–PVP composite for enhanced diagnostic X-ray shielding applications, *J. Inorg. Organomet. Polym. Mater.*, 2023, **33**(8), 2279–2291, DOI: 10.1007/s10904-023-02662-4.

43 H. Liu, Q. Mei, Y. Wang, H. Liu and B. Han, N-vinyl pyrrolidone promoted aqueous-phase dehydrogenation of formic acid over PVP-stabilized Ru nanoclusters, *Science China Chemistry*, 2016, **59**(10), 1342–1347, DOI: 10.1007/s11426-016-0223-0.

44 H. Xia, Y. Hashimoto and T. Hirai, Electric-field-induced actuation of poly (vinyl alcohol) microfibers, *The Journal of Physical Chemistry C*, 2012, **116**(44), 23236–23242, DOI: 10.1021/jp306979c.

45 W. Cao, M. Han, L. Lyu, C. Hu and F. Xiao, Efficient Fenton-like process induced by fortified electron-rich O microcenter on the reduction state Cu-doped CNO polymer, *ACS applied materials & interfaces*, 2019, **11**(18), 16496–16505, DOI: 10.1021/acsami.9b00195.

46 H. Xiang, G. Ren, Y. Zhong, X. Yang, D. Xu, Z. Zhang and X. Wang, Characterization and synthesis of Fe3O4@ C nanoparticles by in-situ solid-phase method, *Mater. Res. Express*, 2021, **8**(2), 025016, DOI: 10.1088/2053-1591/abe21f.

47 H. Zhang and Z. Guo, A superhydrophilic and robust fabric, featuring self-assembled layers of chitosan and carbon nanotubes, facilitates high-throughput oil–water separation, *Sep. Purif. Technol.*, 2024, **344**, 127233, DOI: 10.1016/j.seppur.2024.127233.

48 S. TEETA, R. WANCHANTHUEK, S. SONSUPAP, S. MAENSIRI, N. CHANLEK and K. WONGSAPROM, The Structure and ferromagnetism of carbon nanofibers from polyacrylonitrile/polyvinylpyrrolidone, Journal of Metals, *Materials and Minerals*, 2022, **32**(2), 1–10, DOI: 10.55713/jmmm.v32i2.1250.

49 A. K. Friedman, W. Shi, Y. Losovyj, A. R. Siedle and L. A. Baker, Mapping microscale chemical heterogeneity in Nafion membranes with X-ray photoelectron spectroscopy, *Journal of The Electrochemical Society*, 2018, **165**(11), H733–H741, DOI: **10.1149/2.0771811jes**.

50 K. Molnar, B. Jozsa, D. Barczikai, E. Krisch, J. E. Puskas and A. Jedlovszky-Hajdu, Plasma treatment as an effective tool for crosslinking of electrospun fibers, *J. Mol. Liq.*, 2020, **303**, 112628, DOI: **10.1016/j.molliq.2020.112628**.

51 V. Luque-Agudo, M. Hierro-Oliva, A. M. Gallardo-Moreno and M. L. González-Martín, Effect of plasma treatment on the surface properties of polylactic acid films, *Polym. Test.*, 2021, **96**, 107097, DOI: **10.1016/j.polymertesting.2021.107097**.

52 M. L. Goiana, E. S. de Brito, E. G. Alves Filho, E. de Castro Miguel, F. A. Fernandes, H. M. de Azeredo and M. de Freitas Rosa, Corn starch based films treated by dielectric barrier discharge plasma, *Int. J. Biol. Macromol.*, 2021, **183**, 2009–2016, DOI: **10.1016/j.ijbiomac.2021.05.210**.

53 Z. Sheikhi, L. Mirmoghtadaie, M. R. Khani, M. Farhoodi, S. Beikzadeh, K. Abdolmaleki, F. Kazemian-Bazkiaee, B. Shokri and S. Shojaee-Aliabadi, Physicochemical characterization of argon plasma-treated starch film, *J. Agric. Sci. Technol.*, 2025, **22**(4), 999–1008, **https://dor.isc.ac/dor/20.1001.1.16807073.2020.22.4.9.1**.

54 Q. Lv, T. Xiao, G. Dong, X. Tan, Z. Zhang, M. Zhao, M. Zhu, J. Li and W. Zhang, Preparation and characterization of starch carbamate modified natural sodium alginate composite hydrogel blend formulation and its application for slow-release fertilizer, *Int. J. Biol. Macromol.*, 2024, **278**, 134713, DOI: **10.1016/j.ijbiomac.2024.134713**.

55 Z. Yang, W. Su, J. Fang, Y. Qian and H. Li, A degradable mulch film with fertilizer slow-release function enhanced by lignin, *ACS Appl. Polym. Mater.*, 2023, **5**(9), 6864–6874, DOI: **10.1021/acsapm.3c00904**.

56 S. Kabiri, F. Degryse, D. N. Tran, R. C. da Silva, M. J. McLaughlin and D. Losic, Graphene oxide: a new carrier for slow release of plant micronutrients, *ACS Appl. Mater. Interfaces*, 2017, **9**(49), 43325–43335, DOI: **10.1021/acsami.7b07890**.

57 X. Li, S. Wang, Z. Sun, M. Gao, Q. Li and M. Qin, Study on Enteromorpha Polysaccharide/Konjac Glucomannan Mulch Films with Biochar as a Fertilizer Carrier, *ACS Appl. Polym. Mater.*, 2024, **6**(12), 6946–6956, DOI: **10.1021/acsapm.4c00433**.

58 X. Zhao, J. Lu, S. Jiang, C. Fu, Y. Li, H. Xiang, R. Lu, J. Zhu and B. Yu, Enhancing slow-release performance of biochar-based fertilizers with kaolinite-infused polyvinyl alcohol/starch coating: From fertilizer development to field application, *Int. J. Biol. Macromol.*, 2025, **302**, 140665, DOI: **10.1016/j.ijbiomac.2025.140665**.

59 S. Paliaga, L. Badalucco, V. C. Ciaramitaro, D. F. Martino, A. Gelsomino, E. Kandeler, S. Marhan and V. A. Laudicina, Fertilizer enriched bio-based mulch films increase nitrogen and phosphorus availability and stimulate soil microbial biomass and activity, *Appl. Soil Ecol.*, 2025, **211**, 106159, DOI: **10.1016/j.apsoil.2025.106159**.

60 V. Ciaramitaro, E. Piacenza, S. Paliaga, G. Cavallaro, L. Badalucco, V. A. Laudicina and D. F. Chillura Martino, Exploring the feasibility of polysaccharide-based mulch films with controlled ammonium and phosphate ions release for sustainable agriculture, *Polymers*, 2024, **16**(16), 2298, DOI: **10.3390/polym16162298**.